Chapter

Well Test Analysis for Hydraulically-Fractured Wells

Freddy Humberto Escobar

Abstract

This chapter focuses on the application of Tiab's direct synthesis (*TDS*) technique for practical and accurate interpretation of pressure tests on vertical wells in conventional reservoirs, so bilinear, linear, and elliptical flow regimes can be used for fracture characterization. Most fractured well interpretation tests are conducted using nonlinear regression analysis if the pressure model is available. This method has some drawbacks associated with the nonuniqueness of the solution. Also, the conventional straight-line method requires one plot for each individual flow regime observed in the pressure tests, and the estimated parameters cannot be verified. Tiab's direct synthesis (*TDS*) methodology, which uses specific lines and intersection points found on the pressure and pressure derivative plot, is used in some direct equations which are obtained from the solution of the diffusivity equation for a given flow regime. It has been proven to provide accurate results, and its power allows verification of most results which is not possible from any other technique. The methodology has been successfully explained and tested by its application in two examples, although there exists more than a hundred articles that provide many useful applications.

Keywords: bilinear flow, linear flow, elliptical flow, half-length fracture, fracture conductivity, hydraulic fracturing

1. Introduction

Throughout their history, well test analyses for fractured wells have received many contributions. For practical purposes, let us name the most important ones for this chapter. A good place to start is by mentioning the work in [1], which described the pressure behavior for infinite-conductivity and uniform-flux fractured wells, so people started conducting interpretation tests on such wells by using type-curve matching. Later, [2] introduced the concept of finite-conductivity fractures and established the onset value of dimensionless conductivity as 300. Values lower than that are considered finite-conductivity values, and those above 300 are classified as infinite conductivity. In [2], a fine semi-analytical solution was introduced for describing the well-pressure behavior in hydraulically fractured wells. This solution was then applied in [3] to provide a well interpretation method using type-curve matching. Since then, other mathematical solutions have been presented for finite-conductivity fractures. Among them, the work in [4] using fractal theory is worth mentioning.

The way of conducting well test interpretation was changed by the introduction of Tiab's direct synthesis (TDS) technique by [5]. This revolutionary and modern

technique focuses on the different flow regimes seen on the pressure derivative curve. Defined lines are drawn through each individual flow regime, and the intersection points found among them are read and used for reservoir characterization. Additionally, reading arbitrary points on the pressure and pressure derivative of each flow regime also serve for reservoir parameter determination. A great number of applications of the *TDS* technique are given in [6]. The second work [7], by the same author of [5], presented *TDS* technique for infinite-conductivity and uniform-flux fractures in vertical wells. In [7], the elliptical or biradial flow regime was introduced and characterized. This elliptical flow is also seen in horizontal wells and was characterized in [8–10]. Because of the similarity between the mathematical models of hydraulic fractures and horizontal wells, this concept was applied by [11] to determine the average reservoir pressure in formations drained by horizontal wells using the *TDS* technique. The infinite-conductivity model in [7] also included the late-time pseudosteady-state period as well as some equations involved in the drainage area (conventional analysis for this case was included in [12]). This may be disadvantageous for inexperienced users of *TDS* technique when interpreting pressure tests without reaching reservoir boundaries because the equations involved the use of the unknown reservoir drainage area, although it can be still applied by using the intersection points. To overcome this drawback, [13] presented a new mathematical model excluding the late-time pseudosteady-state period.

TDS technique for finite-conductivity fractured wells is given in [14], with practical field applications to demonstrate the usefulness of the technique. The fracture parameters can be readily obtained by using an arbitrary point on the flow regimes. *TDS* technique plays an important role when analyzing short pressure tests because a user can "make up" nonexisting flow regimes since, for instance, the radial flow horizontal line can be obtained from the reservoir permeability even though radial flow regime is absent. [15, 16] extended the works of finite- and infinite-conductivity fractures in naturally fractured reservoirs. The equations provided by these works can also be applied to either homogeneous or naturally fractured formations since they involve a dummy variable that takes the value of one for the homogeneous case or the value of the dimensionless storativity coefficient for the case of a naturally fractured formation.

TDS technique has also been extended to several scenarios related to hydraulically fractured wells. For instance, when a finite-conductivity fracture intersects with a fault, the pressure trace changes; then, the equations developed in [17] apply for this case. There are cases where a threshold pressure is required to start the flow. The work in [18] includes this concept in uniform-fractured vertical wells, and the work in [19] includes the concept for horizontal wells. Also, when the fractured face is damaged, a pseudolinear flow regime develops along the fracture. [1] included *TDS* technique to characterize such systems. [16] presented *TDS* technique for fractured wells in gas composite reservoirs. *TDS* technique can also be usefully applied to transient-rate analysis, as seen in [20]. Application of *TDS* technique to horizontally isolated fractured wells was presented and characterized in [21] and in conventional analysis in [22]. The works in [23, 24] use *TDS* technique for shale reservoirs. Other applications of *TDS* technique to these systems are given by [25] under transient-rate analysis and [26] for pressure-transient analysis conditions. Other important applications of TDS Technique to fractured wells are given by [29, 30].

This chapter is devoted to the application of *TDS* technique to hydraulically fractured wells in either homogeneous or naturally fractured formations. Without given detailed derivations, the expressions for characterizing the hydraulic fracture parameters are presented along with the way they should be used. Important relationships and practical exercises are included.

2. *TDS* basis

The pioneer publication on the *TDS* technique, [5], explains in detail the derivation of the equations. The Laplace space solution of the arithmetic pressure derivative for a homogeneous and infinite reservoir with skin and wellbore storage is also presented in [5] and given by

$$P_D{}' = \frac{4}{\pi^2}\int_0^\infty \left(\frac{e^{-u^2 t_D}}{u\left\{ \left[uC_D J_0(u) - (1 - C_D s u^2) J_1(u) \right]^2 + \left[uC_D Y_0(u) - (1 - C_D s u^2) Y_1(u) \right]^2 \right\}} \right) du. \tag{1}$$

However, we know that the pressure derivative is a horizontal line during radial flow regime. The dimensionless pressure derivative during radial line is easier represented by

$$t_D{}^* P_D{}' = 0.5. \tag{2}$$

Then, to obtain practical equations, dimensionless parameters must be used. The dimensionless time, based upon half-fracture length and reservoir drainage area, is given below:

$$t_{Dxf} = \frac{0.000263kt}{\phi \mu c_t x_f^2} \tag{3}$$

and

$$t_{DA} = \frac{0.000263kt}{\phi \mu c_t A}. \tag{4}$$

The dimensionless pressure and pressure derivative parameters for oil reservoirs are given by

$$P_D = \frac{kh\Delta P}{141.2q\mu B} \tag{5}$$

and

$$t_D{}^* P_D{}' = \frac{kh(t^* \Delta P')}{141.2q\mu B}. \tag{6}$$

Finally, the dimensionless fracture conductivity introduced in [3] is defined as

$$C_{fD} = \frac{k_f w_f}{k\ x_f}. \tag{7}$$

It is observed from Eq. (5) that the two key parameters of a hydraulic fracture are the half-fracture length, x_f, and the fracture conductivity, $k_f w_f$. The total length of the fracture is given by $2\,x_f$.

The easiest application of *TDS* technique is given by replacing the dimensionless pressure derivative defined by Eqs. (6) and (2), to provide an expression to readily determine formation permeability:

$$k = \frac{70.6q\mu B}{h(t * \Delta P')_R}, \tag{8}$$

where $(t^*\Delta P')_R$ is the pressure derivative value during radial flow regime. The equations for the *TDS* technique are derived in the same manner Eq. (8) was obtained.

3. Biradial flow regime

Biradial or elliptical flow normally results in a hydraulically fractured well when areal anisotropy is present. This is recognized on the pressure derivative versus time log-log plot by a straight line with a slope of 0.36. In hydraulic fractures, the flow from the formation to the fracture is described by parallel flow lines resulting in a linear flow geometry better known as linear flow regime and characterized by a slope of 1/2 on the pressure derivative versus time log-log plot.

Both linear flow and biradial/elliptical flow regimes are seen on the plot of dimensionless pressure and pressure derivative versus dimensionless time based on half-fracture length for a naturally fractured formation. New expressions for the elliptical flow regime introduced in [13] excluding reservoir drainage area are given by.

$$P_D = \frac{25}{9}\left(\frac{\pi t_{Dxf}}{26\xi}\right)^{0.36} \tag{9}$$

and

$$t_D{}^* P_D{}' = \left(\frac{\pi t_{Dxf}}{26\xi}\right)^{0.36}, \tag{10}$$

being ξ a dummy variable that defines either a homogeneous or naturally fractured formation. When $\xi = 1$, a homogeneous reservoir is considered. For the case of naturally fractured formations, $\xi = \omega$, the dimensionless storativity coefficient.

Once dimensionless parameters given by Eqs. (3), (5), and (6) are replaced into Eqs. (9) and (10), respectively, and solve for the half-fracture length, which yields

$$x_f = 22.5632\left(\frac{qB}{h(\Delta P)_{BR}}\right)^{1.3889}\sqrt{\frac{t_{BR}}{\xi\phi c_t}\left(\frac{\mu}{k}\right)^{1.778}} \tag{11}$$

and

$$x_f = 5.4595\left(\frac{qB}{h(t*\Delta P')_{BR}}\right)^{1.3889}\sqrt{\frac{t_{BR}}{\xi\phi c_t}\left(\frac{\mu}{k}\right)^{1.778}}. \tag{12}$$

TDS technique is based on drawing a straight line throughout a given flow regime; then, the user is expected to read the pressure, ΔP_{BR}, and pressure derivative, $(t^*\Delta P')_{BR}$, at a given time, t_{BR}. A better way to reduce noise effects consists of extrapolating the mentioned straight line (biradial for this case) to the time of 1 h and read the pressure derivative value, $(t^*\Delta P')_{BR1}$, at 1 h. For this case, the pressure and pressure derivative set in Eqs. (11) and (12) is changed to ΔP_{BR1} and $(t^*\Delta P')_{BR1}$, respectively.

When bilinear flow is unseen, fracture conductivity can be found with an expression presented in [27]

$$k_f w_f = \frac{3.31739k}{\frac{e^s}{r_w} - \frac{1.92173}{x_f}}. \tag{13}$$

[5] also provided an equation for the determination of the skin factor using an arbitrary point read during radial flow regime:

$$s = 0.5\left\{\frac{\Delta P_R}{(t^*\Delta P')_R} - \ln\left(\frac{kt_R}{\phi\mu c_t r_w^2}\right) + 7.43\right\}. \tag{14}$$

The pseudosteady-state regime governing the pressure derivative equation is given by

$$[t_{DA}{}^*P_D{}']_P = 2\pi(t_{DA})_P. \tag{15}$$

[7] used the point of intersection, t_{RPi}, of Eqs. (2) and (15) to derive an equation for the estimation of the drainage area:

$$A = \frac{kt_{RPi}}{301.77\phi\mu c_t}. \tag{16}$$

The derivation of Eq. (16) follows a similar idea as that presented later in Section 4 for the use of the points of intersection.

4. Bilinear and linear flow regimes

Bilinear flow regime takes place when two linear flows, normal one flowing into the other, take place simultaneously. This situation occurs in low conductivity fractures where linear flow along the fracture and linear flow from the formation to the fracture are observed. Bilinear flow is recognized in the pressure derivative curve by a slope of 0.25. However, this is not shown in **Figure 1** since bilinear flow is absent. The governing expressions for early bilinear and linear flow regimes for vertical fractures in naturally fractured systems were, respectively, presented in [16]

$$P_D = \frac{2.45}{\sqrt{C_{fD}}}\left(\frac{t_{Dxf}}{\xi}\right)^{1/4}, \tag{17}$$

$$t_D{}^*P_D{}' = \frac{0.6125}{\sqrt{C_{fD}}}\left(\frac{t_{Dxf}}{\xi}\right)^{1/4}, \tag{18}$$

$$P_D = \left(\frac{\pi t_{Dxf}}{\xi}\right)^{1/2}, \tag{19}$$

and

$$t_D{}^*P_D{}' = \frac{1}{2}\left(\frac{\pi t_{Dxf}}{\xi}\right)^{1/2}. \tag{20}$$

Linear flow regime can be used to find the half-fracture length, and bilinear flow regime allows finding the fracture conductivity. Once the dimensionless quantities of Eqs. (1) and (3)–(5) are replaced in Eqs. (16)–(19), the fracture conductivity is solved for then

$$k_f w_f = \frac{1947.46}{\sqrt{\xi\phi\mu c_t k}}\left(\frac{q\mu B}{h(\Delta P)_{BL1}}\right)^2, \tag{21}$$

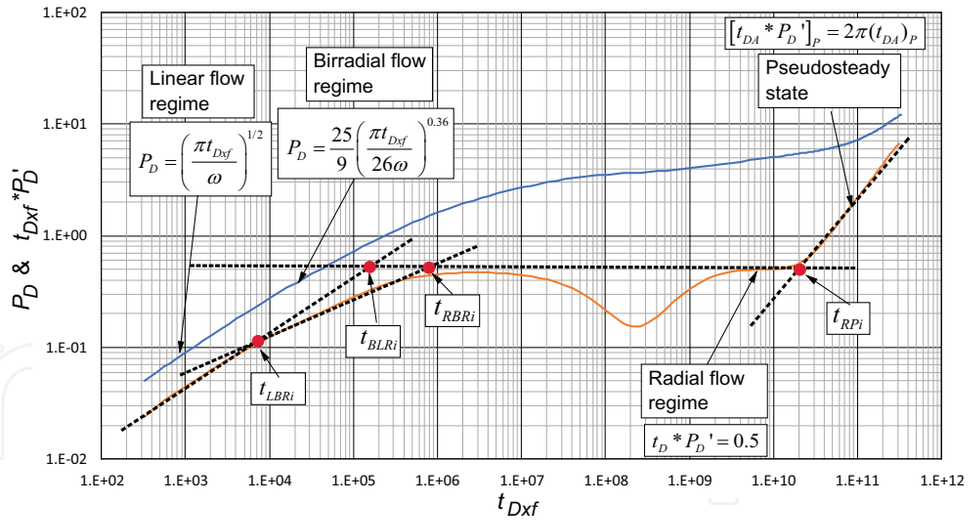

Figure 1.
Dimensionless pressure and pressure derivative behavior for an infinite-conductivity fractured vertical well in a naturally fractured bounded reservoir, $\lambda = 1 \times 10^{-9}$ and $\omega = 0.1$ (taken from [13]).

$$k_f w_f = \frac{121.74}{\sqrt{\xi\phi\mu c_t k}}\left(\frac{q\mu B}{h(t*\Delta P')_{BL1}}\right)^2, \tag{22}$$

Once the fracture conductivity is found, Eq. (7) applies to find the dimensionless fracture conductivity if reservoir permeability and the half-fracture length are known. When bilinear flow is absent, the fracture conductivity may be found from Eq. (13), or the dimensionless fracture conductivity can be read from **Figure 2**:

$$x_f = \frac{4.064qB}{h(\Delta P')_{L1}}\sqrt{\frac{\mu}{\xi\phi c_t k}} \tag{23}$$

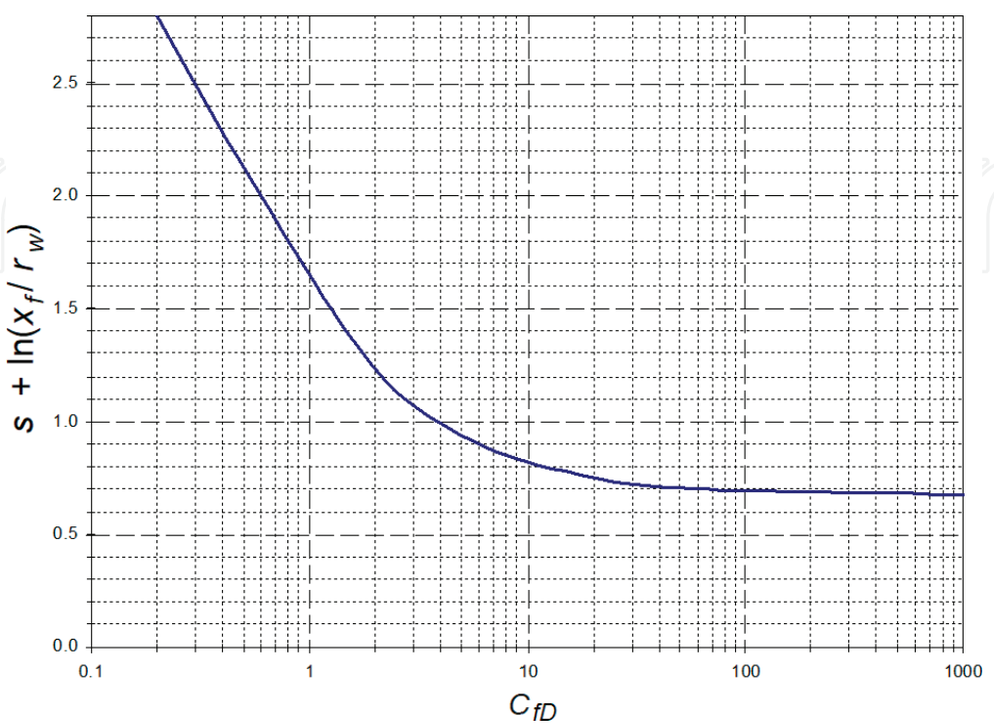

Figure 2.
Effect of skin factor on fracture conductivity (taken from [28]).

and

$$x_f = \frac{2.032qB}{h(t*\Delta P')_{L1}}\sqrt{\frac{\mu}{\xi\phi c_t k}}. \tag{24}$$

5. Points of intersection

If bilinear flow also takes place, then the point of intersection between the pressure derivatives of the bilinear and biradial flow lines, t_{BLBRi}, given by Eqs. (10) and (18), respectively, allows the development of an equation to find the half-fracture as follows:

$$\left(\frac{\pi t_{Dxf}}{26\xi}\right)^{0.36} = \frac{0.6125}{\sqrt{C_{fD}}}\left(\frac{t_{Dxf}}{\xi}\right)^{1/4}. \tag{25}$$

Simplifying,

$$\left(\frac{t_{Dxf}}{\xi}\right)^{0.11} = \frac{0.2862}{\sqrt{C_{fD}}}. \tag{26}$$

Replacing the dimensionless quantities, Eqs. (3) and (7) in Eq. (26) lead to

$$\left(\frac{0.000263kt}{\phi\mu c_t x_f^2 \xi}\right)^{0.11} = 0.2862\sqrt{\frac{k\ x_f}{k_f w_f}}. \tag{27}$$

Solving for the half-fracture from Eq. (27), we readily obtain

$$k_f w_f = 10.5422\left(\frac{\xi\phi\mu c_t k^{3.5454} x_f^{6.5454}}{t_{BRBLi}}\right)^{0.22}. \tag{28}$$

By the same token, the intercept of Eq. (20) with Eq. (18), t_{LBRi}, provides another expression to find the half-fracture length:

$$x_f = \sqrt{\frac{kt_{LBRi}}{39.044\omega\phi\mu c_t}}. \tag{29}$$

Bilinear flow regime is absent in the plot of **Figure 1**. Linear, biradial, and radial flow regimes along with the late pseudosteady-state period are seen. The interception points formed by the possible combinations of such periods can be represented schematically in this plot.

Another way to find the half-fracture length comes from the intersection of Eqs. (2) and (10), t_{RBRi}, and Eq. (10) with Eq. (15), so that

$$x_f = \frac{1}{4584.16}\sqrt{\frac{kt_{RBRi}}{\xi\phi\mu c_t}} \tag{30}$$

and

$$x_f = 41.0554A^{1.3889}\left(\frac{\xi\phi\mu c_t}{kt_{BRPi}}\right)^{0.8889}. \tag{31}$$

The intercept point resulting between linear flow and bilinear flow lines given by the governing pressure derivative solutions, Eqs. (18) and (19), can be used to find either half-fracture length or permeability:

$$k = \left(\frac{k_f w_f}{x_f^2}\right)^2 \frac{16 t'_{BLLi}}{13910 \xi \phi \mu c_t}. \tag{32}$$

t_{BLRi} is the intersection of the bilinear pressure derivative line given by Eq. (18) with the radial flow regime line (Eq. (2)). This intersection point serves as the estimation of either permeability or fracture conductivity:

$$t_{BLRi} = 1677 \frac{\xi \phi \mu c_t}{k^3} \left(k_f w_f\right)^2. \tag{33}$$

6. Other estimations

The expressions for determination of the naturally fractured reservoir parameters cannot be included in this chapter for space reasons. However, they can be found in [15, 16], which also used intersection points and maximum and minimum data read from the pressure and pressure derivative curve.

Radial flow regime may be absent in short tests run in fractured wells with the sole purpose of determining fractured parameters. For these cases, the skin factor can be estimated from any of the two empirical correlations presented by [27]

$$s = \ln\left[r_w\left(\frac{1.92173}{x_f}\right) - \frac{3.31739}{k_f w_f}\right] \tag{34}$$

and

$$s = \ln\frac{r_w}{x_f} + \frac{1.65 - 0.32u + 0.11u^2}{1 + 0.18u + 0.064u^2 + 0.005u^3}, \tag{35}$$

where

$$u = \ln C_{fD}. \tag{36}$$

Additionally, fracture conductivity can be read from the plot given in **Figure 2**.

Finally, space reasons prevent including *TDS* technique for fractured wells in unconventional shale formations. The reader is referred to [23–26].

7. Examples

7.1 Field example

[14] presented a field example of a fractured well test. Pressure and pressure derivative data are given in **Table 1** and **Figure 3**. Other relevant data are provided below:

$$q = 101 \text{ STB/D} \quad \phi = 0.08 \quad \mu = 0.45 \text{ cp}$$

$$c_t = 17.7 \times 10^{-6} \text{ psia}^{-1} \quad B = 1.507 \text{ bbl/STB} \quad h = 42 \text{ ft}$$

$$r_w = 0.28 \text{ ft} \quad t_p = 2000 \text{ h} \quad P_i = 2200 \text{ psia}$$

$$\xi = 1$$

t, h	Δ*P*, psia	*t**Δ*P*', psia	*t*, h	Δ*P*, psia	*t**Δ*P*', psia
0.23	102	26.3	15	390	117
0.39	115	30	20	423	112
0.6	130	35.8	25	446	120
1	145	40.8	30	471	141
1.8	183	57.2	35	493	136.5
2.4	195	67	40	510	132
3.8	260	83.3	45	526	135
4.1	265	69.2	50	540	150
4.96	280	96.9	55	556	137.5
6.2	308	102.3	60	565	144
8.5	320	103.3	65	580	121.1
10	345	149	71	583	

Table 1.
Pressure data for field example (taken from [14]).

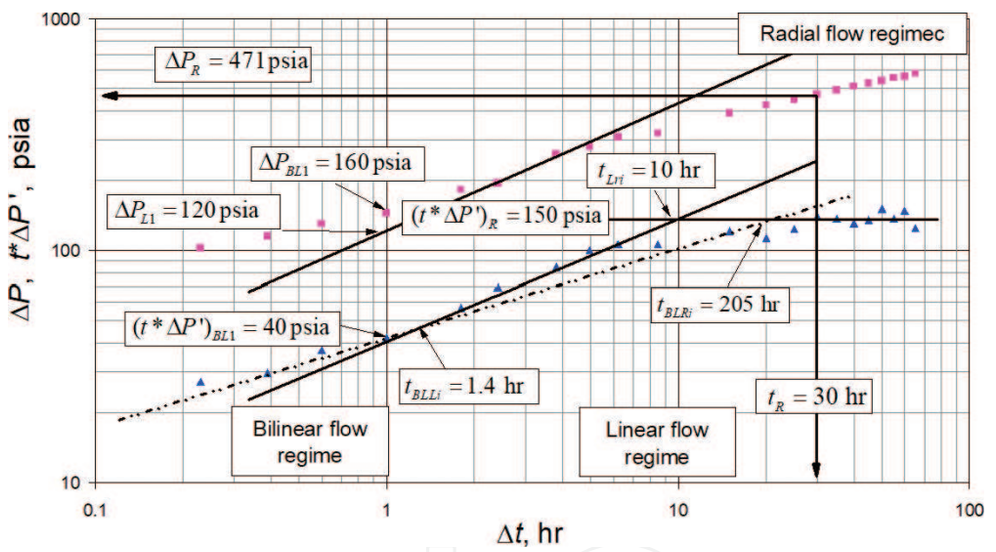

Figure 3.
Pressure and pressure derivative against time log–log plot for field example (taken from [14]).

Using a commercial well test software, the following parameters were estimated by nonlinear regression analysis:

$$k = 0.8 \text{ md}$$

$$xf = 82.2 \text{ ft}$$

$$k_f w_f = 300 \text{ md} - \text{cp}$$

The objective is to compute the hydraulic fracture parameters using the *TDS* technique and compare results obtained from the regression analysis.

7.1.1 Solution

7.1.1.1 Step 1: Obtain the characteristic points

Once the pressure and pressure derivative versus time log-log plot is built and reported in **Figure 3**, the characteristic points are read from such plot as follows:

$$t_R = 30 \text{ h} \quad \Delta P_R = 471 \text{ psia} \quad \left(t^* \Delta P^{'}\right)_R = 150 \text{ psia}$$

$$\left(t^* \Delta P^{'}\right)_{BL1} = 160 \text{ psia} \quad \Delta P_{BL1} = 40 \text{ psia} \quad \Delta P_{L1} = 120 \text{ psia}$$

$$t_{LRi} = 8.2 \text{ h} \quad t_{BLRi} = 195 \text{ h}$$

7.1.1.2 Step 2: Estimate permeability and skin factor

Permeability and skin factor are found in Eqs. (8) and (14) to be 0.76 md and −4.68, respectively.

7.1.1.3 Step 3: Estimate fracture conductivity

Fracture conductivity is estimated using Eqs. (21) and (22):

$$k_f w_f = \frac{121.74}{\sqrt{(0.08)(0.45)\left(17.7 \times 10^{-6}\right)(0.76)}} \left(\frac{(101)(0.45)(1.507)}{(42)(40)}\right)^2 = 290.77 \text{ md-ft}$$

$$k_f w_f = \frac{1947.46}{\sqrt{(0.08)(0.45)\left(17.7 \times 10^{-6}\right)(0.76)}} \left(\frac{(101)(0.45)(1.507)}{(42)(160)}\right)^2 = 290.7 \text{ md-ft.}$$

From **Figure 3**, t_{BLRi} = 200 hr. A very close value is obtained from Eq. (33):

$$t_{BLRi} = 1677 \frac{(0.08)(0.45)\left(17.7 \times 10^{-6}\right)}{(0.76)^3} (290.7)^2 = 205.71 \text{ hr,}$$

which indicates that the calculation of the fracture conductivity is accurate. Notice that instead of estimating t_{BLRi} the fracture conductivity can be found instead to obtain another value of fracture conductivity; then, Eq. (33) can also be expressed as

$$k_f w_f = \sqrt{\frac{k^3 t_{BLRi}}{1677 \xi \phi \mu c_t}} = \sqrt{\frac{0.76^3 (205)}{1677(1)(0.08)(0.45)\left(17.7 \times 10^{-6}\right)}} = 290.2 \text{ md-ft.}$$

7.1.1.4 Step 4: Half-fractured length and dimensionless fracture conductivity estimation

Find half-fracture length with Eqs. (23) and (24):

$$x_f = \frac{4.064(101)(1.507)}{(42)(120)} \sqrt{\frac{0.45}{(0.08)\left(17.7 \times 10^{-6}\right)(0.76)}} = 79 \text{ ft,}$$

$$x_f = \sqrt{\frac{k t_{Lri}}{1207 \xi \phi \mu c_t}} = \sqrt{\frac{(0.76)(10)}{1207(0.08)(0.76)\left(17.7 \times 10^{-6}\right)}} = 76.5 \text{ ft.}$$

Solve for half-fracture length from Eq. (13) and find this:

$$x_f = \frac{1.92173}{\frac{e^s}{r_w} - \frac{3.31739k}{w_f k_f}} = \frac{1.92173}{\frac{e^{-4.6844}}{0.28} - \frac{3.31739(0.76)}{290.7}} = 79 \text{ ft.}$$

Find the dimensionless fracture conductivity using Eq. (5):

$$C_{fD} = \frac{w_f k_f}{x_f k} = \frac{290.7}{79(0.76)} = 4.8.$$

The above value confirms that the fracture has finite conductivity.

7.2 Synthetic example

[13] presented a synthetic example of a pressure test run in a bounded homogeneous reservoir with the information given below:

$$B_o = 1.25 \text{ bbl/STB} \quad q = 300 \text{ STB/D}$$
$$h = 30 \text{ ft} \quad \mu = 5 \text{ cp}$$
$$r_w = 0.3 \text{ ft} \quad c_t = 3 \times 10^{-6} \text{ psi}^{-1}$$
$$P_i = 4000 \text{ psi} \quad \phi = 10\%$$
$$k = 33.334 \text{ md} \quad x_f = 200 \text{ ft}$$
$$A = 592 \text{ Acres}$$

Estimate the half-fracture length by the *TDS* technique, and compare the answer with the value used for generating the test.

7.2.1 Solution

7.2.1.1 Step 1: Obtain the characteristic points.

A pressure and pressure derivative versus time log–log plot is presented in **Figure 4**, from which the following characteristic points are read:

$$t_{BR} = 1.01 \text{ h} \quad \left(t^* \Delta P^{'}\right)_{BR} = 64.63 \text{ psi} \quad t_{BRPi} = 3300 \text{ h}$$

7.2.1.2 Step 2: Half-fractured length estimation.

The half-fracture length is estimated with Eq. (12) and confirmed with Eq. (31), as follows:

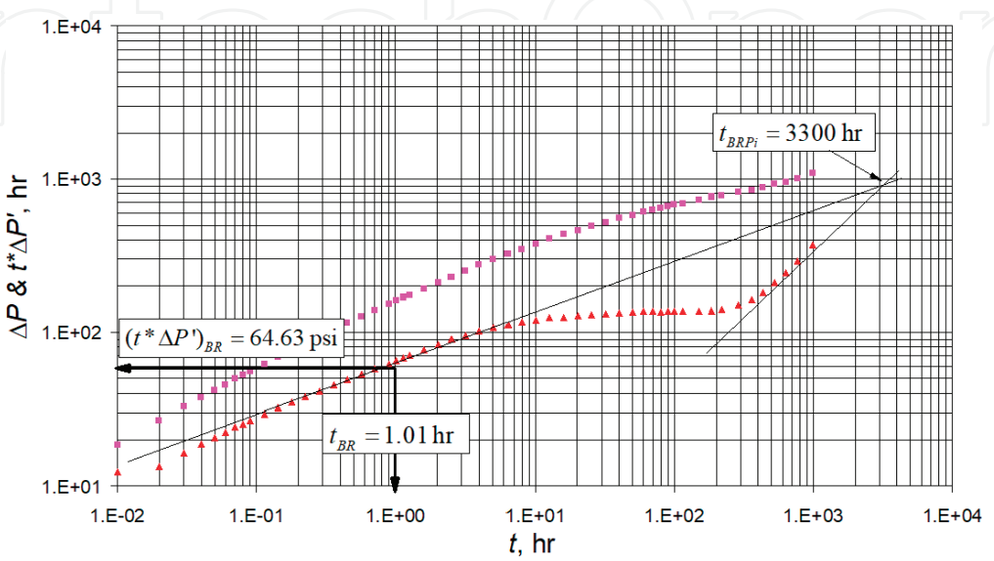

Figure 4.
Pressure and pressure derivative vs. time for synthetic example (taken from [13]).

$$x_f = 5.4595\left(\frac{300(1.25)}{30(64.63)}\right)^{1.3889}\sqrt{\frac{1.01}{(1)(0.1)\left(3\times10^{-6}\right)}\left(\frac{5}{33.334}\right)^{1.778}} = 199 \text{ ft},$$

$$x_f = 41.0554(592\times43560)^{1.3889}\left(\frac{(1)(0.1)(5)\left(3\times10^{-6}\right)}{33.334(3300)}\right)^{0.8889} = 201.6 \text{ ft}.$$

8. Comments on the results

The two given examples show three aspects of the *TDS* technique: (1) practical use, (2) accuracy, and (3) self-confirmation.

As shown in the exercises, the process includes defining flow regimes, drawing a few lines, and finally computing the necessary parameters. Contrary to the conventional straight-line method, which requires a plot for each flow regime, TDS technique uses only the pressure and pressure derivative versus time log-log plot. Computations are straight forward.

Table 2 summarizes the main parameters obtained in the two worked examples. The results show a good agreement between the calculated results by *TDS* technique and the results obtained from commercial software packages, for the field case. The results of the half-fracture length for the synthetic case using *TDS* technique are even better compared to the input value use to simulate the test. This demonstrates that *TDS* technique is an accurate methodology which has been also presented in many publications, not only in the list reference but also in others not mentioned here.

The last aspect dealt with is self-confirmation. In the field example, three values of half-fracture length and three values of fractured conductivity were found, and for the synthetic example, two values of half-fracture length were estimated from different equations. All the estimations match with the reference values.

	Field example						
		Obtained from					
Parameter	Commercial software	Eq. (21)	Eq. (22)	Eq. (33)	Eq. (23)	Eq. (24)	Eq. (13)
x_f, ft	82.2				79	76.5	79
$k_f w_f$, md-ft	300	290.77	290.7	290.2			
	Synthetic example						
		Obtained from					
Parameter	Commercial software	Eq. (12)	Eq. (31)				
x_f, ft	200	199	201.6				

Table 2.
Summary of results.

9. Conclusion

It has been shown that *TDS* technique is a powerful, practical, and accurate tool for well test interpretation because manipulations are easy to do and parameters can be confirmed from different sources from the same pressure test. Compared to reference values, the worked examples provided accurate results of both half-fracture length and hydraulic fracture conductivity. Besides being accurate, *TDS* technique has the great advantage of being able to estimate a given parameter, such

as half-fracture length or fracture conductivity, from more than one source or equation. This provides a means of verifying that the estimated parameter is in a good range.

Acknowledgements

The author wishes to express his gratitude to Universidad Surcolombiana for providing him the time to write this chapter.

Nomenclature

A	Draining area (ft^2)
B	Oil volume factor (rb/STB)
C_{fD}	Dimensionless fracture conductivity
c_t	Compressibility (1/psi)
h	Formation thickness (ft)
k	Formation permeability (md)
$k_f w_f$	Fracture conductivity (md-ft)
P	Pressure (psi)
P_{wf}	Well-flowing pressure (psi)
q	Oil flow rate (STB/D)
q_g	Gas flow rate (MSCF/D)
r_w	Wellbore radius (ft)
x_f	Half-fracture length (ft)
s	Skin factor
t	Test time (h)
t_p	Production time (h)
$t^*\Delta P'$	Pressure derivative (psi)
$t_D{}^*P_D{}'$	Dimensionless pressure derivative

Greek symbols

Δ	Change
ϕ	Porosity (fraction)
λ	Interporosity flow parameter
μ	Viscosity (cp)
ξ	Variable to identify homogeneous (ξ = 1) or heterogeneous ($\xi = \omega$) reservoirs
ω	Dimensionless storativity coefficient

Suffixes

BL	Bilinear
*BL*1	Bilinear at 1 h
BLL	Bilinear-linear intersection
BR	Birradial
*BR*1	Birradial at 1 h
BRBLi	Birradial-bilinear intersection
BRPi	Birradial-pseudosteady intersection
D	Dimensionless
DA	Dimensionless based on area
Dxf	Dimensionless based on half-fractured length
DLBRi	Dual linear-birradial intersection
LBRi	Linear-birradial intersection

R	Radial
RBRi	Radial-birradial intersection
RPi	Intersect of radial-pseudosteady-state lines
w	Well
t	Time
P	Pseudosteady state

Author details

Freddy Humberto Escobar
Universidad Surcolombiana, Neiva, Huila, Colombia

*Address all correspondence to: fescobar@usco.edu.co

References

[1] Gringarten AC, Ramey HJ, Raghavan R. Applied pressure analysis for fractured wells. Journal of Petroleum Technology. Richardson, Texas, USA. 1975:793-800. DOI: 10.2118/5496-PA

[2] Cinco LH, Samaniego VF, Dominguez AN. Transient pressure behavior for a well with a finite-conductivity vertical fracture. SPE Journal. 1978;**18**(4):253-264. DOI: 10.2118/6014-PA

[3] Cinco-Ley H, Samaniego VF. Transient pressure analysis for fractured wells. Journal of Petroleum Technology. 1981; **Sept.**:1479-1766. DOI: 10.2118/7490-PA

[4] Cossio M. A Semi-Analytic Solution for Flow in Finite-Conductivity Vertical Fractures Using Fractal Theory. Richardson, Texas, USA: Society of Petroleum Engineers; 2012. DOI: 10.2118/163057-STU

[5] Tiab D. AAnalysis of pressure and pressure derivative without type-curve Matching: 1-skin and wellbore storage. Journal of Petroleum Science and Engineering. 1995;**12**:171-181. Also Tiab D. Analysis of pressure and pressure derivatives without type-curve matching: i-skin and wellbore storage. Society of Petroleum Engineers. 1993. DOI: 10.2118/25426-MS

[6] Escobar FH. Recent Advances in Practical Applied Well Test Analysis. New York: Nova Science Publishers, Inc.; 2015. 422p

[7] Tiab D. Analysis of pressure derivative without type-curve matching: Vertically fractured wells in closed systems. Journal of Petroleum Science and Engineering. Richardson, Texas, USA. 1994;**11**:323-333. DOI: 10.2118/ 26138-MS. This paper was originally presented as Society of Petroleum Engineers

[8] Escobar FH, Muñoz OF, Sepulveda JA. Horizontal permeability determination from the elliptical flow regime for horizontal wells. CT&F – Ciencia, Tecnología y Futuro. 2004; **2**(5):83-95. ISSN 0122-5383

[9] Escobar FH, Montealegre M. Conventional Analysis for the Determination of the Horizontal Permeability from the Elliptical Flow of Horizontal Wells. Richardson, Texas, USA: Society of Petroleum Engineers; 2007. DOI: 10.2118/105928-MS

[10] Escobar FH, Montealegre-M M. Determination of horizontal permeability from the elliptical flow of horizontal wells using conventional analysis. Journal of Petroleum Science and Engineering. 2008;**61**:15-20. ISSN: 0920-4105

[11] Escobar FH, Cantillo JH, Santos N. A practical approach for the estimation of the average reservoir pressure from multi-rate tests in long horizontal wells. Fuentes: El Reventón Energético. 2011; **9**(1):13-20

[12] Escobar FH, Montealegre MM, Cantillo JH. Conventional analysis for characterization of bi-radial (elliptical) flow in infinite-conductivity vertical fractured wells. CT&F – Ciencia, Tecnología y Futuro. 2006;**3**(2):141-147

[13] Escobar FH, Ghisays-Ruiz A, Bonilla LF. New model for elliptical flow regime in hydraulically-fractured vertical wells in homogeneous and naturally-fractured systems. Journal of Engineering and Applied Sciences. 2014;**9**(9):1629-1636

[14] Tiab D, Azzougen A, Escobar FH, Berumen S. Analysis of Pressure Derivative Data of Finite-Conductivity Fractures by the "Direct Synthesis" Technique. Society of Petroleum Engineers; 1999. DOI: 10.2118/52201-MS

[15] Escobar FH, Zhao YL, Fahes M. Characterization of the naturally fractured reservoir parameters in infinite-conductivity hydraulically-fractured vertical wells by transient pressure analysis. Journal of Engineering and Applied Science. 2015; **10**(12):5352-5362

[16] Tiab D, Bettam Y. Practical Interpretation of Pressure Tests of Hydraulically Fractured Wells in a Naturally Fractured Reservoir. Richardson, Texas, USA: Society of Petroleum Engineers; 2007. DOI: 10.2118/107013-MS

[17] Escobar FH, Tiab D, Berumen-Campos S. Well Pressure Behavior of a Finite-Conductivity Fracture Intersecting a Finite Sealing-Fault. Richardson, Texas, USA: Society of Petroleum Engineers; 2003. DOI: 10.2118/80547-MS

[18] Escobar FH, Zhao YL, Pournik M, Liu QG, Olaya-Marin G. Interpretation of pressure tests in uniform-flux fractured vertical wells with threshold pressure gradient in low permeability reservoirs. Journal of Engineering and Applied Science. 2015;**10**(20):9364-9372

[19] Escobar FH, Zhao YL, Zhang LH. Interpretation of pressure tests in horizontal wells in homogeneous and heterogeneous reservoirs with threshold pressure gradient. Journal of Engineering and Applied Sciences. 2014;**9**(11):2220-2228

[20] Escobar FH, Castro JR, Mosquera JS. Rate-transient analysis for hydraulically fractured vertical oil and gas wells. Journal of Engineering and Applied Science. 2014;**9**(5):739-749. ISSN: 1819-6608

[21] Al Rbeawi SJH, Tiab D. Effect of the Number and Length of Zonal Isolations on Pressure Behavior of Horizontal Wells. Society of Petroleum Engineers; 2011. DOI: 10.2118/142177-MS

[22] Escobar FH, Meneses AR, Losada LM. Straight-line conventional transient pressure analysis for horizontal wells with isolated zones. Dynamis. 2014; **81**(185):78-85

[23] Bernal KM, Escobar FH, Ghisays-Ruiz A. Pressure and pressure derivative analysis for hydraulically-fractured shale formations using the concept of induced permeability field. Journal of Engineering and Applied Science. 2014; **9**(10):1952-1958

[24] Escobar FH, Montenegro LM, Bernal KM. Transient-rate analysis for hydraulically-fractured gas shale wells using the concept of induced permeability field. Journal of Engineering and Applied Science. 2014; **9**(8):1244-1254

[25] Escobar FH, Rojas JD, Ghisays-Ruiz A. Transient-rate analysis for hydraulically-fractured horizontal wells in naturally-fractured shale gas reservoirs. Journal of Engineering and Applied Science. 2015;**10**(1):102-114

[26] Escobar FH, Bernal KM, Olaya-Marin G. Pressure and pressure derivative analysis for fractured horizontal wells in unconventional shale reservoirs using dual-porosity models in the stimulated reservoir volume. Journal of Engineering and Applied Sciences. 2014;**9**(12):2650-2669

[27] Tiab D. Advances in Pressure Transient Analysis — TDS Technique. Lecture Notes Manual. Norman, Oklahoma, USA: The University of Oklahoma; 2003. 577p

[28] Economides MJ, Watters, Dunn-Norman S. Petroleum Well Construction. New York: John Wiley & Sons; 1988. 622p

[29] Escobar FH, Gonzalez RA, Hernandez LM, Hernandez CM. Pressure and pressure derivative analysis for hydraulically fractured

vertical wells with face skin. Journal of Engineering and Applied Science. 2016; **11**(13):8268-8273

[30] Zhao YL, Escobar FH, Hernandez CM, Zhang CP. Performance analysis of a vertical well with a finite-conductivity fracture in gas composite reservoirs. Journal of Engineering and Applied Sciences. 2016;**11**(15):8992-9003